Journal of Power Sources 188 (2009) 387–396

Contents lists available at ScienceDirect

Journal of Power Sources

journal homepage: www.elsevier.com/locate/jpowsour

Osmium–ruthenium carbonyl clusters as methanol tolerant electrocatalysts for oxygen reduction

E. Borja-Arco [a], R.H. Castellanos [b], J. Uribe-Godínez [a], A. Altamirano-Gutiérrez [a], O. Jiménez-Sandoval [a,*]

[a] Centro de Investigación y de Estudios Avanzados del Instituto Politécnico Nacional (Cinvestav), Unidad Querétaro, Apartado Postal 1-798, Querétaro, Qro. 76001, Mexico
[b] Universidad del Papaloapan, Campus Tuxtepec, Circuito Central No. 2000, Col. Parque Industrial, Tuxtepec, Oax. 68301, Mexico

ARTICLE INFO

Article history:
Received 13 October 2008
Received in revised form 4 December 2008
Accepted 5 December 2008
Available online 11 December 2008

Keywords:
Osmium
Ruthenium
Electrocatalyst
Oxygen reduction
Proton exchange membrane fuel cell
Direct methanol fuel cell

ABSTRACT

This work presents the synthesis and the structural and electrochemical characterization of novel mixed $Os_xRu_y(CO)_n$ electrocatalysts for oxygen reduction in 0.5 mol L^{-1} H_2SO_4; their monometallic $Os_x(CO)_n$ and $Ru_y(CO)_n$ counterparts were synthesized as well, for comparison purposes. The catalysts were obtained by thermolysis of $Ru_3(CO)_{12}$ and $Os_3(CO)_{12}$ (either alone or mixed) in three organic solvents: 1,2-dichlorobenzene (b.p. 178–180 °C), *n*-nonane (b.p. 150–151 °C) and *o*-xylene (b.p. 143–145 °C), under reflux conditions. The products were characterized by FT-IR spectroscopy and scanning electronic microscopy, and their chemical composition obtained by energy-dispersive X-ray spectroscopy. The electrocatalytic activity of the new materials was evaluated by room temperature RDE measurements, using the cyclic and linear sweep voltammetry techniques; all of them are methanol tolerant ORR catalysts, however, the bimetallic clusters, in general, show more favorable characteristics to perform this reaction than their monometallic analogues. On this basis, the novel catalysts can be considered as potential candidates to be used as cathodes in PEMFCs and DMFCs.

1. Introduction

Direct methanol fuel cells (DMFCs) are important energy production devices with advantages over typical H_2/air proton exchange membrane fuel cells (PEMFCs) for certain applications; thus, they do not require a reformer to operate and possess all the advantages of using a liquid, low cost and highly available fuel. However, DMFCs exhibit a relatively low performance when compared to hydrogen fuel cells. This fact has been mainly attributed to two reasons: (1) the slower kinetics of the methanol oxidation reaction, and (2) the important degree of permeation of the methanol fuel to the cathode compartment through the polymer membrane of the DMFC (*crossover effect*); the methanol molecules crossing the membrane are oxidized on the Pt based catalysts usually employed on the cathode to perform the oxygen reduction reaction (ORR), and the competition between such two electrochemical processes results in an important performance loss of the cell [1–3]. Two solutions are mainly envisaged for the second problem: the use of polymer membranes less permeable to methanol between both electrodes and/or the use of methanol tolerant (inactive) cathode electrocatalysts. The first issue has been explored with limited satisfactory results [4,5]. As regards cathode catalysts for fuel cells, Pt based materials are the most widely used to date due to their relatively high activity for the oxygen reduction reaction, however, as mentioned above, they are active to methanol as well [3,6]. Relatively few cathode catalysts have been reported to show different degrees of resistance to methanol, namely: Pt-Fe [3] and Pt-Se [7] systems; Ru based materials, mostly containing Se and/or Mo atoms [8–11]; Os based clusters [12], as well as some mono- and bimetallic transition metal porphyrins [13–15]. Most of these materials, however, have been reported to tolerate methanol concentrations not higher than 1.0 mol L^{-1}.

In this work, we present a new class of bimetallic osmium–ruthenium carbonyl cluster compounds, *i.e.* $Os_xRu_y(CO)_n$, which are able to perform the oxygen reduction reaction in 0.5 mol L^{-1} H_2SO_4, even in the presence of 2.0 mol L^{-1} methanol solutions. Such properties render the new materials potential candidates to be used as cathodes in PEMFCs and as methanol resistant cathodes in direct methanol fuel cells (DMFCs). For the sake of comparison, the corresponding monometallic carbonyl compounds (*i.e.* $Os_x(CO)_n$ and $Ru_y(CO)_n$, respectively) have been synthesized as well.

2. Experimental

2.1. Preparation and structural characterization of the catalysts

The novel $Os_xRu_y(CO)_n$ electrocatalysts were synthesized by reaction of equal number of moles of triosmium dodecacarbonyl [$Os_3(CO)_{12}$, Aldrich] and triruthenium dodecacarbonyl [$Ru_3(CO)_{12}$,

* Corresponding author. Tel.: +52 442 2119903; fax: +52 442 2119938.
E-mail address: ojimenez@qro.cinvestav.mx (O. Jiménez-Sandoval).

0378-7753/$ – see front matter © 2008 Elsevier B.V. All rights reserved.
doi:10.1016/j.jpowsour.2008.12.021

Aldrich] in three organic solvents (*o*-xylene, b.p. 143-145 °C; *n*-nonane, b.p. 150–151 °C; and 1,2-dichlorobenzene, b.p. 178–180 °C) at their reflux temperatures (all from Aldrich and used as received). Two different kinds of products were obtained from the syntheses in 1,2-dichlorobenzene and *o*-xylene: (1) an insoluble material, separated by centrifuging the reaction mixture, and (2) a solid product obtained by evaporation of the latter; in contrast, only one kind of product was obtained from the reaction in *n*-nonane, an insoluble material, also recovered by centrifugation. In all cases, the blackish powders obtained were washed with diethyl ether (J.T. Baker) and dried at room temperature. The structural characterization of the new materials was performed by means of diffuse reflectance FT-IR spectroscopy, on a PerkinElmer-GX3 spectrometer, with the samples dissolved in FT-IR grade KBr. A Philips XL30ESEM microscope was used to obtain scanning electron micrographs and energy-dispersive X-ray spectra (EDS) of the catalysts, for surface morphology and chemical composition studies, respectively.

On the other hand, the corresponding *monometallic* carbonyl clusters, *i.e.* $Os_x(CO)_n$ and $Ru_y(CO)_n$, were synthesized under the same conditions employed for the bimetallic carbonyls, for comparison purposes. The syntheses with $Os_3(CO)_{12}$ yielded two kinds of products, an insoluble material and a solid obtained by evaporation of the reaction mixture; the syntheses with $Ru_3(CO)_{12}$, by contrast, produced only an insoluble material. All the monometallic products were characterized by the same structural and electrochemical techniques as their bimetallic counterparts.

2.2. Electrode preparation

The working electrode for the rotating disk electrode (RDE) studies was prepared by mixing 1.5 mg of Vulcan® XC-72 (Cabot) and 0.5 mg of the catalyst with 10 μL of a 5% Nafion® solution (ElectroChem) in an ultrasonic bath; 1.5 μL of the resulting mixture were deposited on a glassy carbon disk electrode and dried at room temperature. The cross-section (geometrical) area of the disk electrode was 0.072 cm^2.

2.3. Electrochemical experiments

2.3.1. Equipment

The RDE studies were carried out at 25 °C in a conventional electrochemical cell with a water jacket, with three compartments for the working, counter and reference electrode, respectively. A mercury sulfate electrode ($Hg/Hg_2SO_4/0.5\ mol\ L^{-1}\ H_2SO_4$; abbreviated as MSE) was used as reference (MSE = 0.680 V/NHE), however, the potential values reported are referred to the normal hydrogen electrode (NHE); a salt bridge was used to avoid contamination of the reference electrode due to the presence of methanol during the electrochemical studies. A carbon cloth was used as counter electrode. The 0.5 mol L^{-1} H_2SO_4 electrolyte used in these studies was prepared with 98% sulfuric acid (J.T. Baker) and deionized water (18.2 MΩ-cm). A potentiostat/galvanostat (Princeton Applied Research, model 263A) and a PC with Echem-M270 software were used for the electrochemical measurements. A Radiometer Analytical BM-EDI101 glassy carbon rotating disk electrode (with a CTV101 speed control unit) was used for the voltammetry studies.

2.3.2. Methods

2.3.2.1. In the absence of methanol. Cyclic voltammetry (CV) experiments were done to clean, activate and characterize the electrode surface. Prior to each CV measurement, the electrolyte was purged with nitrogen (Infra; UHP) for 30 min. The electrode was subjected to 35 potential sweeps between 0 and 0.98 V/NHE, at a 20 mV s^{-1} rate. In the case of the studies of 30%Pt/Vulcan® XC-72 electrodes, performed for reference, the potential sweeps were done in the 0-1.58 V/NHE range, at a 50 mV s^{-1} rate. The open circuit potential ($E_{oc}^{N_2}$) was measured at the end of each potential scan. The temperature of the system was maintained at 25 °C.

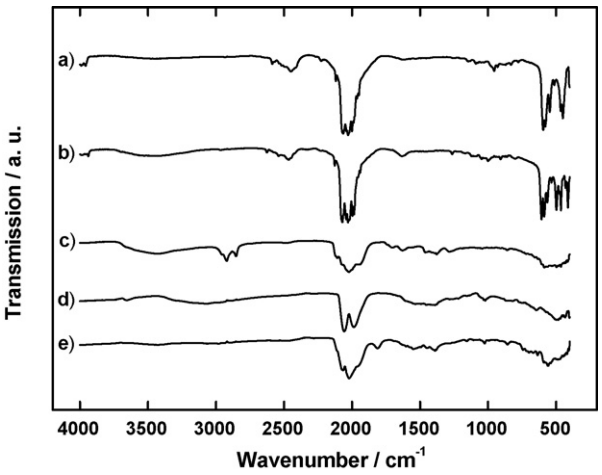

Fig. 1. FT-IR spectra of: (a) $Ru_3(CO)_{12}$; (b) $Os_3(CO)_{12}$. Representative FT-IR spectra of: (c) the monometallic osmium catalysts, $Os_x(CO)_n$; (d) the monometallic ruthenium catalysts, $Ru_y(CO)_n$; (e) the bimetallic $Os_xRu_y(CO)_n$ electrocatalysts.

Linear sweep voltammetry (LSV) measurements were performed to study the oxygen reduction reaction on the new materials and on 30%Pt/Vulcan® XC-72 as reference, at 25 °C. The electrolyte was saturated with oxygen (Infra; UHP) for 15 min. The open circuit potential ($E_{oc}^{O_2}$) was measured for each catalyst. Polarization curves were obtained in the $E_{oc}^{O_2}$ to 0 V/NHE range for the new materials and in the $E_{oc}^{O_2}$ to 0.2 V/NHE range for Pt, at a 5 mV s^{-1} rate. Rotation rates ranged from 100 to 900 rpm. Measurements were performed at least three times for each material.

2.3.2.2. In the presence of methanol. Once the ORR studies in the absence of methanol were finished, the same electrolyte was purged with pure N_2 for 20 min and CV measurements were performed: two potential sweeps between 0 and 0.98 V/NHE, at a 20 mV s^{-1} rate for the novel materials, and between 0 and 1.58 V/NHE, at a 50 mV s^{-1} rate for Pt. Absolute methanol (J.T. Baker) was then added to the electrolyte so as to reach a final CH_3OH concentration of 1.0 or 2.0 mol L^{-1}; CV measurements (two potential scans under the above conditions) were subsequently made to detect possible current peaks associated to methanol oxidation.

LSV curves were obtained in order to study the performance of the new materials and Pt as ORR electrocatalysts in the presence of methanol (1.0 and 2.0 mol L^{-1}), under the same conditions as those described in Section 2.3.2.1. Measurements were performed at least three times for each material.

3. Results and discussion

3.1. Structural characterization

Fig. 1 shows representative FT-IR spectra of the novel $Os_xRu_y(CO)_n$ electrocatalysts and their monometallic Os and Ru counterparts, as well as those of the $Os_3(CO)_{12}$ and $Ru_3(CO)_{12}$ precursors as references. The spectra of the starting materials (Fig. 1a and b) show strong carbonyl stretching vibration bands, in the 1940–2130 cm^{-1} range, as well as a group of bands around 570 cm^{-1}, which have been assigned to carbonyl deformation modes, $\delta_{M\text{-}CO}$ [16]. It is interesting to note that *all* the materials synthesized in this work (both bi- and monometallic) show carbonyl stretching bands around 2030 cm^{-1} (Fig. 1c–e), in contrast to, for example, ORR osmium electrocatalysts obtained in *n*-octane [17] and ruthenium catalysts prepared in different atmospheres (in the absence of solvents) [18], which virtually lose all the

Table 1
Chemical composition of the $Os_xRu_y(CO)_n$ electrocatalysts determined by EDS.

Element (wt%)	Synthesis solvent[a]			Synthesis solvent[b]	
	1,2-Dichlorobenzene	*n*-Nonane	*o*-Xylene	1,2-Dichlorobenzene	*o*-Xylene
C	14.53	16.78	20.25	36.96	27
O	12.21	19.07	17.52	14.36	16.44
Os	43.39	27.95	25.62	33.23	46.68
Ru	29.9	36.21	36.62	3.22	9.89
Cl				12.24	

[a] Insoluble materials.
[b] Materials obtained by evaporation of the reaction mixture.

carbonyl groups present in the corresponding precursor reagent. Table 1 shows the chemical composition of the bimetallic catalysts, in agreement with these observations. On the other hand, particular features observed in some of the spectra are the bands at *ca.* 2850 and 2920 cm^{-1} for both of the monometallic $Os_x(CO)_n$ products prepared in *o*-xylene (an example of which is shown in Fig. 1c), as well as the bimetallic material obtained from the 1,2-dichlorobenzene solution (not shown); in addition, these materials show a weaker signal around 1450 cm^{-1}; such two groups of bands, which fall within the C–H stretching and C–C ring vibration ranges of substituted benzenes, respectively [19], could be an indicative of the π coordination of aromatic molecules from the solvent to some metal centers of the complexes, considering the strong affinity of aromatic rings for ruthenium and osmium carbonyl clusters [20,21]. Another particular feature, in the case of the spectrum of the $Os_xRu_y(CO)_n$ electrocatalyst obtained from the *o*-xylene reaction

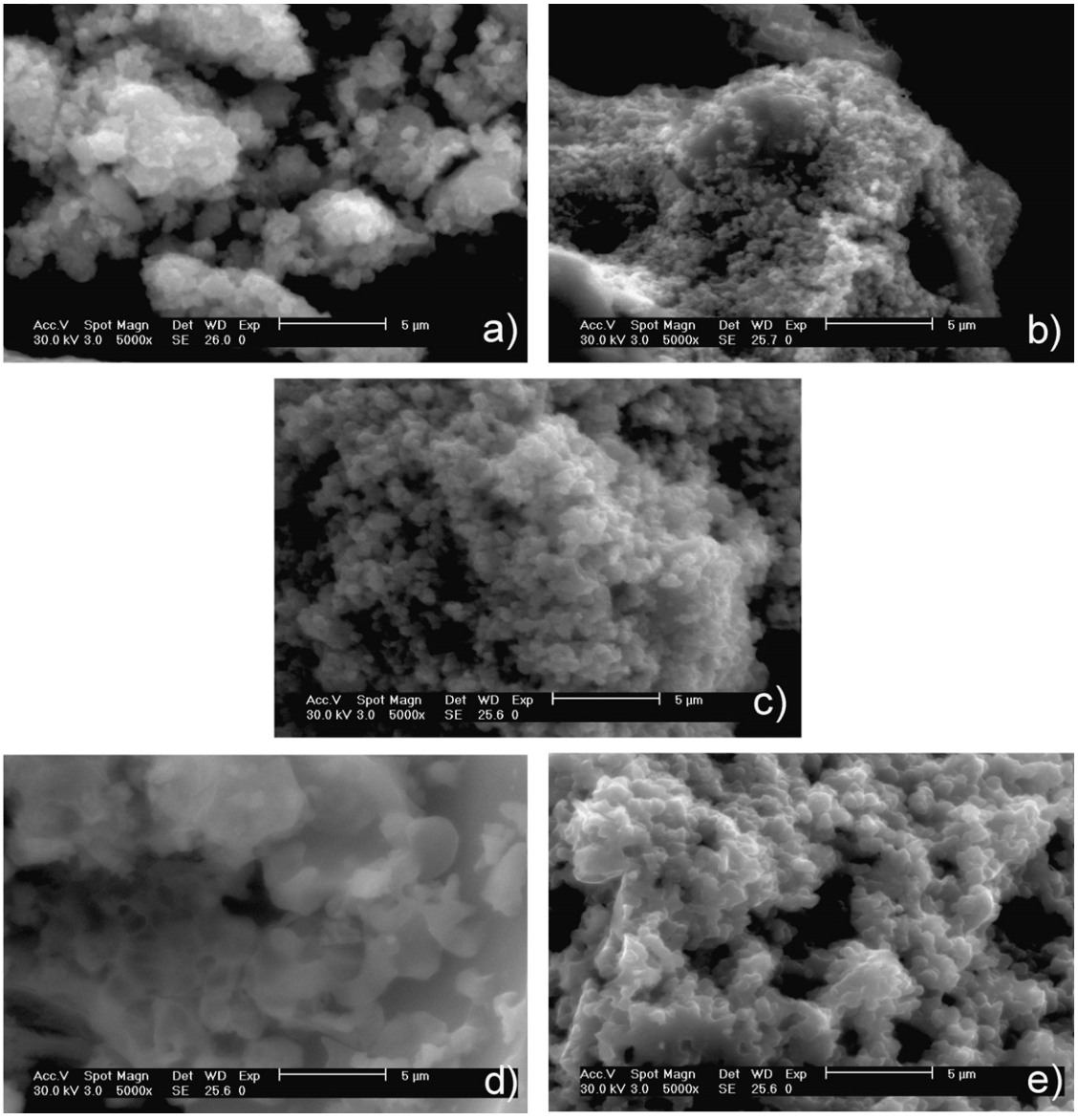

Fig. 2. Scanning electron micrographs of the $Os_xRu_y(CO)_n$ electrocatalysts insoluble in the reaction mixture: (a) 1,2-dichlorobenzene; (b) *n*-nonane; (c) *o*-xylene. Scanning electron micrographs of the $Os_xRu_y(CO)_n$ electrocatalysts obtained by evaporation of the reaction mixture: (d) 1,2-dichlorobenzene; (e) *o*-xylene.

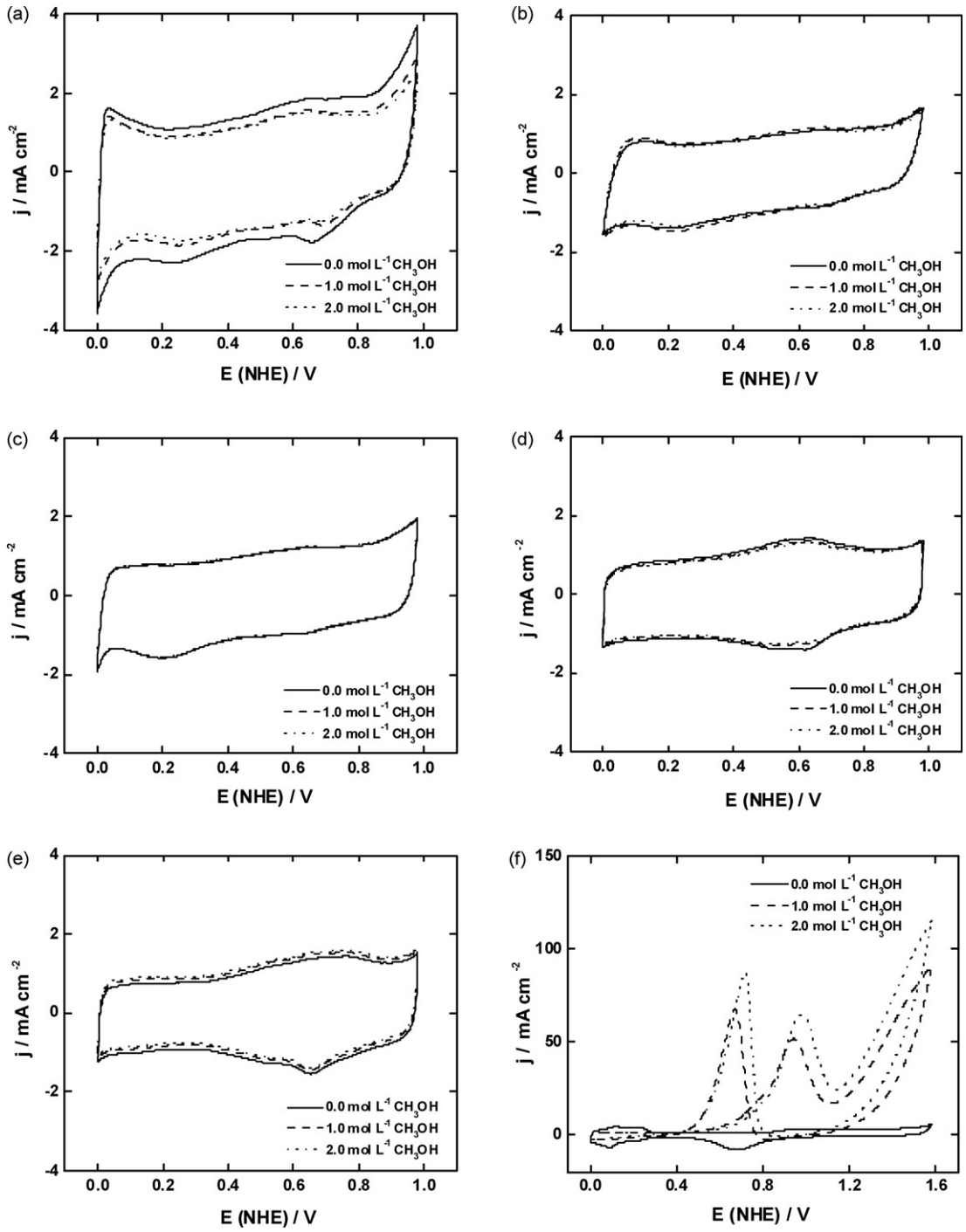

Fig. 3. Cyclic voltammograms of the $Os_xRu_y(CO)_n$ electrocatalysts insoluble in the reaction mixture: (a) 1,2-dichlorobenzene; (b) *n*-nonane; (c) *o*-xylene. Cyclic voltammograms of the $Os_xRu_y(CO)_n$ electrocatalysts obtained by evaporation of the reaction mixture: (d) 1,2-dichlorobenzene; (e) *o*-xylene. (f) Cyclic voltammograms of 30%Pt/Vulcan® XC-72. In all cases, the corresponding voltammograms in the presence of 1.0 and 2.0 mol L^{-1} methanol solutions are included. The electrolyte was 0.5 mol L^{-1} H_2SO_4 and the sweep rate 20 mV/s for the $Os_xRu_y(CO)_n$ electrocatalysts and 50 mV/s for Pt.

solution, is the small, but well defined band observed at 1816 cm^{-1} (Fig. 1e); this band may probably be attributed to the presence of bridge carbonyl groups (or a single group), which are usually observed at smaller frequencies than their terminal counterparts [22]; the presence of a bridging CO ligand in this material could be understood in terms of the condensation/rearrangement reactions that clusters of the $M_3(CO)_{12}$ type used in this work usually undergo in pyrolysis conditions [20–22].

Fig. 2 shows the SEM images of the $Os_xRu_y(CO)_n$ electrocatalysts obtained under different conditions. All the materials exhibit similar sponge-like surface morphologies, which can be an advantageous property for their use as catalysts. The particle cluster size is, however, somewhat larger for the materials recovered on evaporating the reaction mixture.

3.2. Electrochemical characterization

3.2.1. Cyclic voltammetry

Fig. 3 shows the cyclic voltammograms for the new bimetallic ORR electrocatalysts, in the absence and presence of 1.0 and

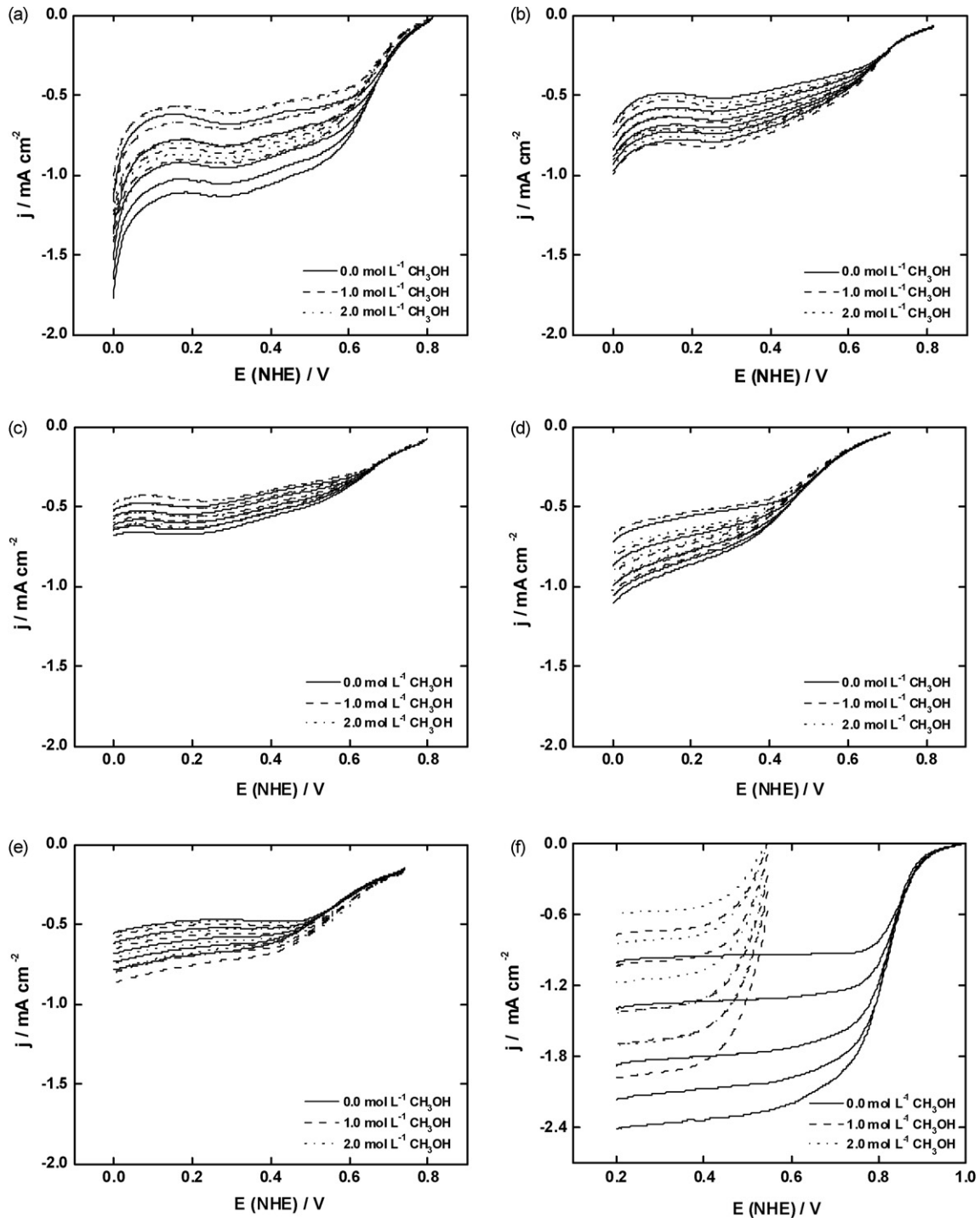

Fig. 4. ORR current–potential curves for the $Os_xRu_y(CO)_n$ electrocatalysts insoluble in the reaction mixture: (a) 1,2-dichlorobenzene; (b) *n*-nonane; (c) *o*-xylene. ORR current–potential curves for the $Os_xRu_y(CO)_n$ electrocatalysts obtained by evaporation of the reaction mixture: (d) 1,2-dichlorobenzene; (e) *o*-xylene. (f) ORR current–potential curves for 30%Pt/Vulcan® XC-72. In all cases, the corresponding curves in the presence of 1.0 and 2.0 mol L^{-1} methanol solutions are included. The electrolyte was 0.5 mol L^{-1} H_2SO_4 and the sweep rate 5 mV/s.

2.0 mol L^{-1} methanol solutions, as well as for 30%Pt/Vulcan® XC-72 as reference. It can be observed that, in agreement with the chemical compositions reported in Table 1, the cyclic voltammograms of the catalysts deposited as solids from the reaction mixtures show a cathodic peak at 0.15–0.3 V/NHE, as well as anodic–cathodic peaks in the 0.5–0.85 V/NHE range (Fig. 3a–c), which indicate the presence of ruthenium [18] and osmium [17], respectively; such metals may have been formed during the syntheses, in amounts small enough to be undetected by X-ray diffraction measurements. The Ru cathodic peak could be due to the presence of some residual ruthenium oxides, RuO_x [23,24], and, since no other Ru peaks are observed, the carbonyl groups attached to the ruthenium atoms are apparently protecting them from oxidation, at least within the potential range studied. Similar considerations may apply in the case of the Os metal centers of the clusters, since no other peaks are observed apart from those in the 0.5–0.85 V/NHE range mentioned above, attributed to redox processes exhibited by osmium metal nanoparticles [17]. A similar protective effect

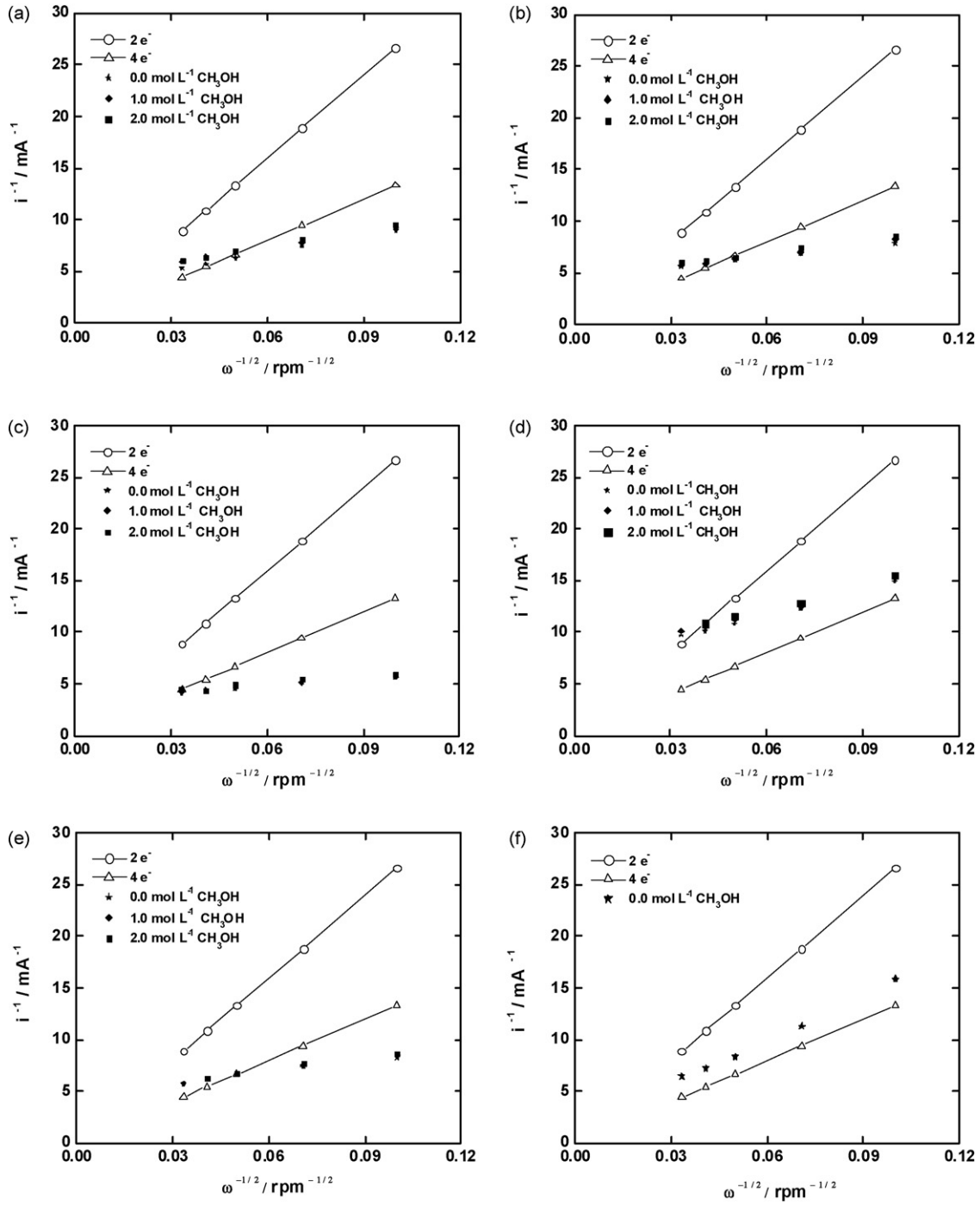

Fig. 5. Experimental (at 0.4 V/NHE) and theoretical (2 and 4 electrons) Koutecky-Levich plots for the $Os_xRu_y(CO)_n$ electrocatalysts insoluble in the reaction mixture: (a) 1,2-dichlorobenzene; (b) *n*-nonane; (c) *o*-xylene. Experimental (at 0.4 V/NHE) and theoretical (2 and 4 electrons) Koutecky-Levich plots for the $Os_xRu_y(CO)_n$ electrocatalysts obtained by evaporation of the reaction mixture: (d) 1,2-dichlorobenzene; (e) *o*-xylene. In all cases, the corresponding plots in the presence of 1.0 and 2.0 mol L^{-1} methanol solutions are included. (f) Experimental (at 0.4 V/NHE) and theoretical (2 and 4 electrons) Koutecky-Levich plots for 30%Pt/Vulcan® XC-72.

of carbonyl ligands on ruthenium based oxygen reduction electrocatalysts has been discussed by Tributsch et al. [8]. Another feature observed in these voltammograms is the presence of hydrogen and oxygen evolution peaks, in the cathodic 0-0.1 V/NHE and anodic 0.85–1.0 V/NHE region, respectively; such processes are specially favored on the insoluble bimetallic material obtained in 1,2-dichlorobenzene (Fig. 3a).

As for the bimetallic materials obtained by evaporation of the reaction mixture, their cyclic voltammograms (Fig. 3d and e), in contrast with those of the insoluble materials (Fig. 3a–c), practically show only osmium cathodic–anodic peaks, in the 0.55–0.85 V/NHE range; no peaks that could be ascribed to ruthenium were observed. This behavior is in agreement with the chemical composition of these materials (Table 1), which exhibit a clear predominance of osmium over ruthenium.

A remarkable feature of the cyclic voltammograms of both kinds of bimetallic catalysts, soluble as well as insoluble in the reaction solution, is that they remained practically unchanged in the presence of 1.0 and 2.0 mol L^{-1} methanol aqueous solutions; in neither case were the methanol oxidation peaks observed [25,26];

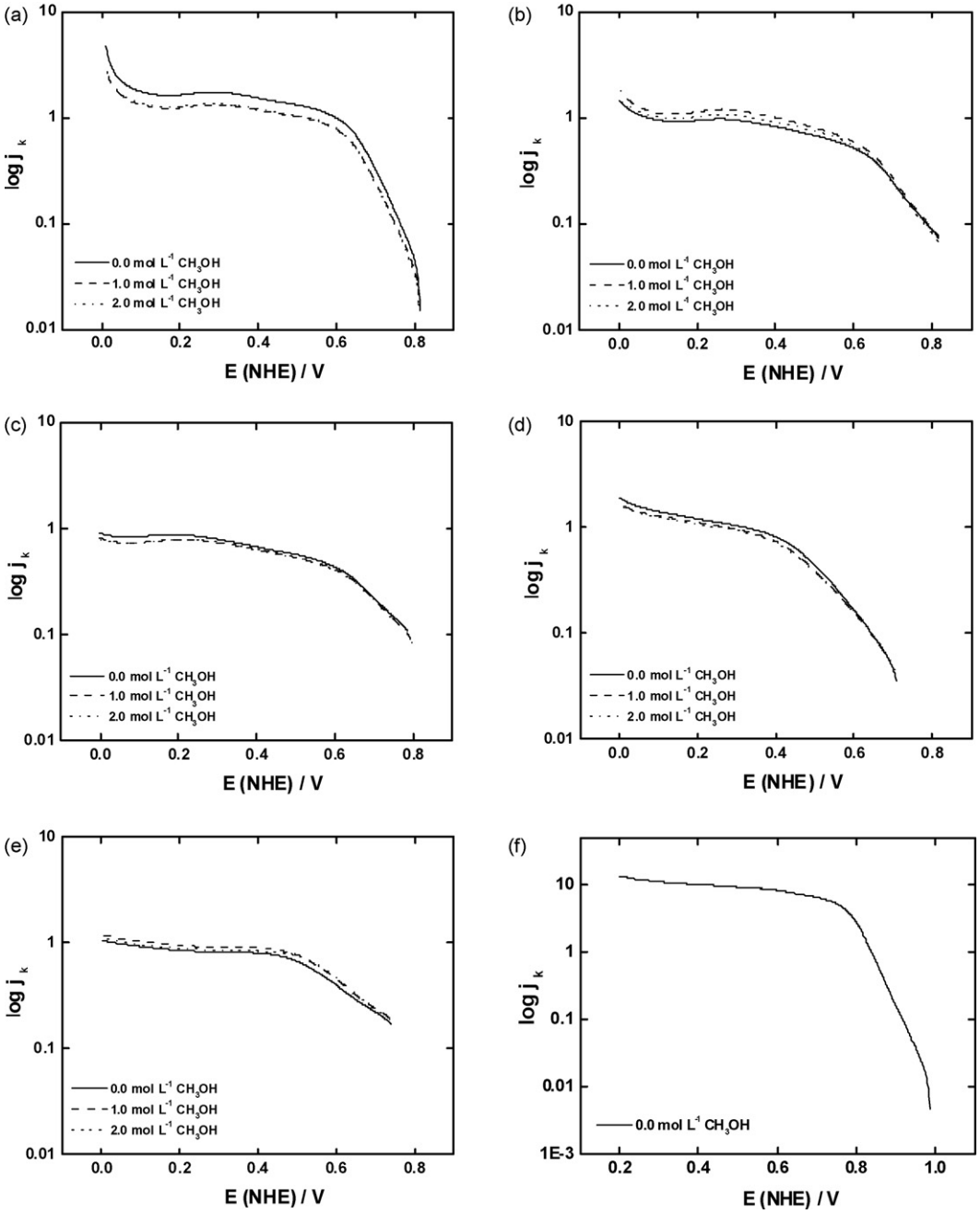

Fig. 6. ORR mass-corrected Tafel plots for the $Os_xRu_y(CO)_n$ electrocatalysts insoluble in the reaction mixture: (a) 1,2-dichlorobenzene;(b) *n*-nonane; (c) *o*-xylene. ORR mass-corrected Tafel plots for the $Os_xRu_y(CO)_n$ electrocatalysts obtained by evaporation of the reaction mixture: (d) 1,2-dichlorobenzene; (e) *o*-xylene. In all cases, the corresponding plots in the presence of 1.0 and 2.0 mol L^{-1} methanol solutions are included. f) ORR mass-corrected Tafel plots for 30%Pt/Vulcan® XC-72.

this could be considered as a first sign of the important methanol tolerance degree exhibited by the new materials. In contrast, the 30%Pt/Vulcan® catalyst shows very sharp methanol oxidation peaks, indicating its high activity for this process.

3.2.2. Linear sweep voltammetry: oxygen reduction reaction

Typical current–potential curves of the bimetallic electrocatalysts in the presence and absence of methanol aqueous solutions are presented in Fig. 4, along with those of 30%Pt/Vulcan® XC-72 as reference. These curves show the three distinct regions characteristic of ORR processes taking place on a catalyst's surface: (I) the kinetic region, where the current, i_k, is independent of the rotation velocity; (II) the mixed control region, where the behavior is determined by kinetic as well as diffusion processes; and (III) the mass-transfer region, where the diffusion current, i_d, is a function of the rotation velocity. However, in the latter region, due to the presence of a peak at ~0.3 V/NHE, the insoluble bimetallic materials do not show a well defined diffusion plateau (Fig. 4a–c); such peak is not observed for the bimetallic materials obtained by evaporation of the reaction mixture (Fig. 4d and e). These features are in agreement with the corresponding cyclic voltammograms (Fig. 3) and chemical compositions (Table 1) of both kinds of materials, *i.e.* the peak at ~0.3 V/NHE (associated with the presence of ruthenium) is not evident in the materials where osmium is clearly predominant. Furthermore, the inclination of the curves with the rotation speed has been previously observed for catalyzed irreversible electrode processes [14].

Table 2
Open circuit potential values and ORR kinetic parameters of the $Os_xRu_y(CO)_n$ electrocatalysts in O_2-saturated 0.5 mol L^{-1} H_2SO_4, at 25 °C.

Synthesis solvent	$[CH_3OH]$ (mol L^{-1})	$E^{O_2}_{OC}$ V/NHE	b (mV decade^{-1})	α	$j_o \times 10^{-5}$ mA cm^{-2}
	0	0.815	128.65	0.4601	2.02
1,2-Dichlorobenzene[a]	1.0	0.815	130.66	0.4529	2.05
	2.0	0.815	132.37	0.4475	2.00
	0	0.814	215.05	0.2752	85.5
n-Nonane[a]	1.0	0.816	207.40	0.2853	68.9
	2.0	0.814	206.66	0.2863	62.8
	0	0.791	276.36	0.2143	276.5
o-Xylene[a]	1.0	0.796	267.99	0.2209	238
	2.0	0.799	270.04	0.2192	238.5
	0	0.704	219.02	0.2702	21.16
1,2-Dichlorobenzene[b]	1.0	0.708	237.79	0.2489	33.20
	2.0	0.702	250.86	0.2362	48.52
	0	0.737	365.17	0.1622	800
o-Xylene[b]	1.0	0.735	346.65	0.1708	700
	2.0	0.735	350.72	0.1691	711.5
30%Pt/C	0	0.990	78.12	0.7574	1.07

[a] Insoluble materials.
[b] Materials obtained by evaporation of the reaction mixture.

For all cases, however, the most important feature of the polarization curves is that they are practically unchanged by the presence of 1.0 and 2.0 mol L^{-1} methanol solutions with both kinds of bimetallic materials, *i.e.* these materials are tolerant to the presence of this fuel cell contaminant to a very important extent. In sharp contrast, however, the Pt electrode exhibits a mixed potential due to the simultaneous methanol oxidation and oxygen reduction reactions on its surface [27], which in turn caused the net cathodic current onset to shift negatively by *ca.* 0.5 V/NHE (Fig. 4f).

It has been established that in order to obtain the total electrocatalytic activity of a material for the ORR, the kinetic and diffusion currents must be known. The Koutecky-Levich equation at a given potential is

$$\frac{1}{i} = \frac{1}{i_k} + \frac{1}{i_d} \tag{1}$$

where i is the measured disk current, i_k the kinetic current, and i_d the diffusion controlled current. This equation may be used to separate i_k from i_d, and get the real electrocatalyst activity [28]. For the rotating disk electrode experiment, in the laminar flow regime, the diffusion current is a function of the rotation velocity and hence, Eq. (1) may be written as

$$\frac{1}{i} = \frac{1}{i_k} + \frac{B}{\omega^{1/2}} \tag{2}$$

where ω is the electrode rotation velocity in rpm and B is a constant given by [29]:

$$B = \left(\frac{1}{200nFA\nu^{-1/6}D_{O_2}^{2/3}C_{O_2}} \right) \tag{3}$$

where n is the number of electrons exchanged per mol of O_2, F the Faraday constant, A the catalytic effective surface area, ν the kinematic viscosity of the electrolyte, D_{O_2} the oxygen diffusion coefficient and C_{O_2} the bulk oxygen concentration in the electrolyte; the values used in this work were 0.01 cm^2 s^{-1} for the kinematic viscosity, 1.4×10^{-5} cm^2 s^{-1} for the oxygen diffusion coefficient and 1.1×10^{-6} mol cm^{-3} for the bulk oxygen concentration [30]. According to Eq. (2), a plot of $1/i$ *vs.* $1/\omega^{1/2}$ for various potentials should yield straight and parallel lines with intercepts corresponding to the inverse of the real kinetic current, i_k, and slopes yielding the values of B. The number of electrons transferred in the oxygen reduction reaction can be assessed with the values of B, according to Eq. (3). Fig. 5 shows the theoretical (with $n = 2$ and 4; A = electrode geometric area, 0.072 cm^2) and experimental Koutecky-Levich plots at two different methanol concentrations, at a given potential value (0.4 V/NHE). An important observation is that, in general, the bimetallic catalysts show plots that resemble closer the curves calculated for a $n = 4$ process, than those for a two electron process (Fig. 5a–e); this suggests that O_2 is most likely reduced to H_2O, following a direct, four electron pathway at the solid electrode/solution interface. Similar results were obtained for the 30%Pt/Vulcan® electrodes, but in the absence of methanol (Fig. 5f).

On this basis, the effective catalytic surface area, A_{eff}, can be calculated from Eq. (3), using the experimental Koutecky-Levich slope, B_{exp}, and $n = 4$:

$$A_{eff} = \frac{1}{200nFB_{exp}\nu^{-1/6}D_{O_2}^{2/3}C_{O_2}} \tag{4}$$

All the currents measured (cyclic voltammograms, polarization curves and Tafel plots) were normalized to this effective area.

All the materials synthesized showed linear $1/i$ *vs.* $1/\omega^{1/2}$ plots, which can be associated with a first order reaction with respect to the oxygen dissolved in the electrolyte [30,31]; moreover, such linearity is not affected by the presence of methanol.

Normally, the kinetic current values obtained from the interception of the Koutecky-Levich plots are used to generate the Tafel curves ($\log i_k$ *vs.* E); however, very precise results may not be obtained due to inevitable variations in the experimental conditions. For this reason, the current–potential curves were corrected by a previously described procedure [29], in order to get the correct kinetic current:

$$i_k = \frac{i \cdot i_d}{i_d - i} \tag{5}$$

The mass transport corrected Tafel plots ($\log[i \cdot i_d/(i_d - i)]$ *vs.* E) for the oxygen reduction reaction, obtained using Eq. (5), are shown in Fig. 6. In agreement with the previous electrochemical results, the form of the curves is basically the same, regardless of the presence of methanol (Fig. 6a–e). The Tafel plot obtained for the Pt electrode in the absence of methanol is provided as reference as well (Fig. 6f).

The kinetic parameters (obtained from the Tafel plots) and open circuit potentials ($E^{O_2}_{oc}$) of the bimetallic electrocatalysts are presented in Table 2, along with those of 30%Pt/Vulcan® XC-72. The kinetic parameters and open circuit potentials ($E^{O_2}_{oc}$) of the

Table 3
Open circuit potential values and ORR kinetic parameters of the $Ru_y(CO)_n$ electrocatalysts in O_2-saturated 0.5 mol L^{-1} H_2SO_4, at 25 °C.

Synthesis solvent	$[CH_3OH]$ (mol L^{-1})	$E^{O_2}_{OC}$ V/NHE	b (mV decade^{-1})	α	$j_o \times 10^{-5}$ mA cm^{-2}
1,2-Dichlorobenzene	0	0.763	181.48	0.3264	20.75
	1.0	0.763	183.22	0.3236	21.40
	2.0	0.763	181.61	0.3259	17.20
n-Nonane	0	0.824	131.51	0.4505	2.47
	1.0	0.824	131.03	0.4516	2.35
	2.0	0.824	130.30	0.4544	2.30
o-Xylene	0	0.800	176.91	0.3349	23.20
	1.0	0.800	174.64	0.3392	17.70
	2.0	0.800	174.65	0.3386	17.60

monometallic materials are shown in Tables 3 and 4 for comparison purposes.

It can be observed that all the bimetallic catalysts show open circuit potentials ($E^{O_2}_{OC}$) above 0.7 V/NHE, however, the highest values ($\geq$ *ca.* 0.8 V/NHE) are exhibited by the insoluble materials, *i.e.* those where the weight percentages of ruthenium and osmium are comparable; the catalysts obtained from the reaction solution, where osmium is predominant, show the lowest $E^{O_2}_{OC}$ values. In agreement with these results, the monometallic $Ru_y(CO)_n$ catalysts show open circuit potentials (Table 3) higher than those of the $Os_x(CO)_n$ materials (Table 4). The insoluble $Os_xRu_y(CO)_n$ materials, moreover, show higher $E^{O_2}_{OC}$ values than all the osmium monometallic catalysts and the ruthenium monometallic catalyst prepared in 1,2-dichlorobenzene; the open circuit potentials, however, are comparable in the case of the $Ru_y(CO)_n$ catalysts synthesized in *n*-nonane and *o*-xylene.

On the other hand, Tafel slopes considerably different from that of platinum are observed for most of the bi- and monometallic materials, which suggests that they follow different reaction pathways [32]; other authors consider that Tafel slopes higher than 120 mV decade^{-1} are related to the presence of some adsorbed oxides on the electrode surface [24]; this consideration is not likely to apply to the present materials, at least not to an important extent, since their major components are the metal carbonyls, the metal particles being present only in small amounts.

As for the charge transfer coefficient (α), the bimetallic catalyst with the highest value (0.46), *i.e.* that with the largest decrease of reaction free energy [33], was that synthesized in 1,2-dichlorobenzene, close to the behavior exhibited by platinum. Similar values were obtained for the monometallic $Ru_y(CO)_n$ catalyst prepared in *n*-nonane. Remarkably, the α values exhibited by these materials are not significantly modified by the presence of methanol in the electrolyte.

The exchange current density (j_o) is one of the most important kinetic parameters of the ORR, since it is proportional to its constant rate (k) [29]; the $Os_xRu_y(CO)_n$ catalysts recovered from the reaction solution (soluble materials) exhibit higher exchange current densities ($\sim 10^{-4}$ mA cm^{-2}) than their insoluble counterparts ($\sim 10^{-5}$–10^{-4} mA cm^{-2}) and platinum ($\sim 10^{-5}$ mA cm^{-2}), as expected from their Tafel slopes. The highest j_o values ($\sim 10^{-3}$ mA cm^{-2}) are exhibited by the two materials obtained in *o*-xylene, which, accordingly, show the highest values of b. When these materials are compared with the monometallic catalysts prepared in the same solvent, the former show higher exchange current densities, with the exception of the insoluble $Os_xRu_y(CO)_n$ catalyst synthesized in 1,2-dichlorobenzene. When compared with other monometallic Ru [9] and Os [12,34,35] carbonyl complexes reported in the literature, the present bimetallic clusters also show higher exchange current density values, in the 10^{-3}–10^{-5} mA cm^{-2} range, in comparison with the j_o values of the order of 10^{-5} and 10^{-6} mA cm^{-2} for the former. This fact is very significant, considering the direct relation of this parameter with the velocity of the oxygen reduction reaction, *i.e.* the importance of the presence of both types of metal atoms for the electrocatalytic activity of the carbonyl cluster is clearly evidenced here. It is also interesting to note that the exchange current densities of these materials are also

Table 4
Open circuit potential values and ORR kinetic parameters of the $Os_x(CO)_n$ electrocatalysts in O_2-saturated 0.5 mol L^{-1} H_2SO_4, at 25 °C.

Synthesis solvent	$[CH_3OH]$ (mol L^{-1})	$E^{O_2}_{OC}$ V/NHE	b (mV decade^{-1})	α	$j_o \times 10^{-5}$ mA cm^{-2}
1,2-Dichlorobenzene[a]	0	0.707	193.81	0.3060	12.52
	1.0	0.707	206.97	0.2867	19.45
	2.0	0.707	216.75	0.2736	25.20
n-Nonane[a]	0	0.642	209.84	0.2825	12.15
	1.0	0.642	221.92	0.2670	19.65
	2.0	0.642	242.64	0.2447	30.80
o-Xylene[a]	0	0.750	167.49	0.3552	11.08
	1.0	0.750	176.33	0.3366	15.30
	2.0	0.750	182.74	0.3242	17.95
1,2-Dichlorobenzene[b]	0	0.777	193.32	0.3061	38.40
	1.0	0.777	194.99	0.3035	30.70
	2.0	0.777	187.88	0.3149	29.20
n-Nonane[b]	0	0.670	258.63	0.2288	45.30
	1.0	0.670	266.75	0.2218	48.20
	2.0	0.660	284.83	0.2077	65.90
o-Xylene[b]	0	0.752	245.48	0.2407	54.30
	1.0	0.752	266.61	0.2217	72.70
	2.0	0.752	281.46	0.2102	103

[a] Insoluble materials.
[b] Materials obtained by evaporation of the reaction mixture.

higher than those of most methanol resistant and non-resistant ORR electrocatalysts reported in the literature [9,12,17,30,35–38].

4. Conclusions

Novel bimetallic Os–Ru electrocatalysts for the oxygen reduction reaction have been prepared in this work, and their behavior compared with monometallic Os and Ru materials prepared and studied under the same conditions. All the materials contain carbonyl ligands in their structure, which is a novelty in an area where metal nanoparticles are the dominating materials; such ligands are likely to exert a protective effect on the metal centers of the complexes against oxidation, a feature in favor of their electrocatalytic activity. All the materials prepared, both bi- and monometallic, perform the ORR reaction with an activity comparable or higher than those exhibited by other catalysts reported in the literature. In addition, all of them are tolerant even to 2.0 mol L^{-1} methanol solutions, a concentration commonly used in DMFCs, in contrast to most methanol resistant catalysts reported to date, which exhibit a 1.0 mol L^{-1} tolerance upper limit. Such characteristics render the new materials potential candidates to be used as cathodes in PEMFCs and DMFCs, without showing the negative effects of platinum in the presence of methanol. The analysis of the open circuit potentials and kinetic parameters, with special emphasis on the exchange current density, indicates that the combination of Os and Ru is favorable for the catalytic properties of the materials for the ORR, *i.e.* a synergistic effect of both metals is being observed.

Acknowledgements

The authors wish to thank J. Márquez-Marín, R.A. Mauricio-Sánchez and J.E. Urbina-Alvarez for valuable technical assistance. Partial financial support (through grant no. 52280) and graduate scholarships (to E. Borja-Arco, J. Uribe-Godínez and A. Altamirano-Gutiérrez) from CONACYT (National Council of Science and Technology, Mexico) are also acknowledged.

References

[1] X. Li, Principles of Fuel Cells, Taylor & Francis, New York, 2006, pp. 513–517.
[2] M.P. Hogarth, T.R. Ralph, Platinum Met. Rev. 46 (2002) 146–164.
[3] A.K. Shukla, R.K. Raman, Annu. Rev. Mater. Res. 33 (2003) 155–168.
[4] O. Savadogo, J. Power Sources 127 (2004) 135–161.
[5] J. Ling, O. Savadogo, J. Electrochem. Soc. 151 (2004) A1604–A1610.
[6] Z. Jusys, R.J. Behm, Electrochim. Acta 49 (2004) 3891–3900.
[7] R.-F. Wang, S.-J. Liao, H.-Y. Liu, H. Meng, J. Power Sources 171 (2007) 471–476.
[8] H. Tributsch, M. Bron, M. Hilgendorff, H. Schulenburg, I. Dorbandt, V. Eyert, P. Bogdanoff, S. Fiechter, J. Appl. Electrochem. 31 (2001) 739–748.
[9] A.L. Ocampo, R.H. Castellanos, P.J. Sebastian, J. New Mater. Electrochem. Syst. 5 (2002) 163–168.
[10] T.J. Schmidt, U.A. Paulus, H.A. Gasteiger, N. Alonso-Vante, R.J. Behm, J. Electrochem. Soc. 147 (2000) 2620–2624.
[11] N. Alonso-Vante, P. Bogdanoff, H. Tributsch, J. Catal. 190 (2000) 240–246.
[12] R.H. Castellanos, A.L. Ocampo, P.J. Sebastian, J. New Mater. Electrochem. Syst. 5 (2002) 83–90.
[13] G.Q. Sun, J.T. Wang, R.F. Savinell, J. Appl. Electrochem. 28 (1998) 1087–1093.
[14] R. Jiang, D. Chu, J. Electrochem. Soc. 147 (2000) 4605–4609.
[15] D. Chu, R. Jiang, Solid State Ionics 148 (2002) 591–599.
[16] C.E. Anson, U.A. Jayasooriya, Spectrochim. Acta 46A (1990) 861–869.
[17] J. Uribe-Godínez, R.H. Castellanos, E. Borja-Arco, A. Altamirano-Gutiérrez, O. Jiménez-Sandoval, J. Power Sources 177 (2008) 286–295.
[18] R.H. Castellanos, E. Borja-Arco, A. Altamirano-Gutiérrez, R. Ortega-Borges, Y. Meas, O. Jiménez-Sandoval, J. New Mater. Electrochem. Syst. 8 (2005) 69–75.
[19] D. Lin-Vien, N.B. Colthup, W.G. Fateley, J.G. Grasselli, The Handbook of Infrared and Raman Characteristic Frequencies of Organic Molecules, Academic Press, San Diego, 1991.
[20] P.J. Dyson, B.F.G. Johnson, C.M. Martin, Coord. Chem. Rev. 155 (1996) 69–86.
[21] G.R. Knox, Organometallic Compounds of Ruthenium and Osmium (Chapman and Hall Chemistry Sourcebooks), Springer, New York, 1998.
[22] F.A. Cotton, G. Wilkinson, Advanced Inorganic Chemistry, fourth ed., Interscience Publishers, Chichester, 1998.
[23] H. Schulenburg, M. Hilgendorff, I. Dorbandt, J. Radnik, P. Bogdanoff, S. Fiechter, M. Bron, H. Tributsch, J. Power Sources 155 (2006) 47–51.
[24] N.A. Anastasijević, Z.M. Dimitrijević, R.R. Adžić, Electrochim. Acta 31 (1986) 1125–1130.
[25] Z. Liu, Z. Qun Tian, S. Ping Jiang, Electrochim. Acta 52 (2006) 1213–1220.
[26] C.L. Campos, C. Roldán, M. Aponte, Y. Ishikawa, C.R. Cabrera, J. Electroanal. Chem. 581 (2005) 206–215.
[27] K. Lee, O. Savadogo, A. Ishihara, S. Mitsushima, N. Kamiya, K. Ota, J. Electrochem. Soc. 153 (2006) A20–A24.
[28] V.Y. Filinovsky, Y.V. Pleskov, Rotating Disk and Ring-Disk Electrodes, New York Consultants Bureau, New York, 1976.
[29] E. Gileadi, Electrode Kinetics, VCH Publishers, New York, 1993.
[30] N. Alonso-Vante, H. Tributsch, O. Solorza-Feria, Electrochim. Acta 40 (1995) 567–576.
[31] A. Damjanovic, M.A. Genshaw, J.O'M. Bockris, J. Electrochem. Soc. 114 (1967) 1107–1112.
[32] E. Yeager, J. Mol. Catal. 38 (1986) 5–25.
[33] A.J. Bard, L.R. Faulkner, Electrochemical Methods, John Wiley & Sons, New York, 2001.
[34] R.H. Castellanos, R. Rivera-Noriega, O. Solorza-Feria, J. New Mater. Electrochem. Syst. 2 (1999) 85–88.
[35] R.H. Castellanos, A.L. Ocampo, J. Moreira-Acosta, P.J. Sebastian, Int. J. Hydrogen Energy 26 (2001) 1301–1306.
[36] M. Pattabi, R.H. Castellanos, R. Castillo, A.L. Ocampo, J. Moreira, P.J. Sebastian, J.C. McClure, X. Mathew, Int. J. Hydrogen Energy 26 (2001) 171–174.
[37] O. Solorza-Feria, S. Durón, Int. J. Hydrogen Energy 27 (2002) 451–455.
[38] J.M. Ziegelbauer, V.S. Murthi, C. O'Laoire, A.F. Gullá, S. Mukerjee, Electrochim. Acta 53 (2008) 5587–5596.